Supplementary Materials: Interpolation of GPS and Geological Data Using InSAR Deformation Maps: Method and Application to Land Subsidence in the Alto Guadalentín Aquifer (SE Spain)

Marta Béjar-Pizarro, Carolina Guardiola-Albert, Ramón P. García-Cárdenas, Gerardo Herrera, Anna Barra, Antonio López Molina, Serena Tessitore, Alejandra Staller, José A. Ortega-Becerril and Ramón P. García-García

Table S1. Location and velocity of GPS sites (see map in Figure 1b).

Site Number	Longitude	Latitude	Date1	Date2	v (cm/Year)
1	−1722	37,646	20090301	20130128	−4
2	−1691	37,680	20090301	20130301	−2
3	−1639	37,696	20040907	20130213	−2
4	−1694	37,662	20050317	20130128	−5
5	−1689	37,654	20050317	20130222	−11
6	−1683	37,645	20050317	20130211	−12
7	−1678	37,637	20050317	20130222	−10
8	−1673	37,627	20050317	20130222	−9
9	−1658	37,601	20050316	20130213	−2
10	−1652	37,592	20050316	20130213	−1
11	−1647	37,584	20050316	20130213	−1
12	−1643	37,576	20050316	20130205	−2
13	−1638	37,568	20050316	20130222	−1
14	−1691	37,673	20050317	20130128	−3
15	−1715	37,652	20090301	20130128	−4
16	−1708	37,659	20090301	20130128	−4
17	−1672	37,686	20040907	20130301	−2
18	−1650	37,693	20040907	20130301	−2
19	−1700	37,685	20040821	20130221	0
20	−1704	37,694	20040821	20130220	0
21	−1708	37,703	20040820	20130220	0
22	−1707	37,711	20040820	20130220	0
23	−1712	37,728	20040820	20130205	0
24	−1627	37,699	20040906	20130214	−2
25	−1616	37,703	20040906	20130214	−3
26	−1605	37,706	20040906	20130214	−2
27	−1584	37,716	20040903	20130214	−2
28	−1572	37,721	20040903	20130214	−2
29	−1728	37,640	20090301	20130221	−3
30	−1736	37,633	20090301	20130221	−4
31	−1743	37,625	20090301	20130221	−5
32	−1750	37,618	20090301	20130205	−3
33	−1562	37,726	20040902	20130215	−3
34	−1551	37,731	20040902	20130215	−2
35	−1545	37,733	20040902	20130215	−1
36	−1534	37,739	20040902	20130215	−1
37	−1525	37,743	20040901	20130215	−1
38	−1516	37,749	20040901	20130220	−1
39	−1509	37,757	20040901	20130205	0

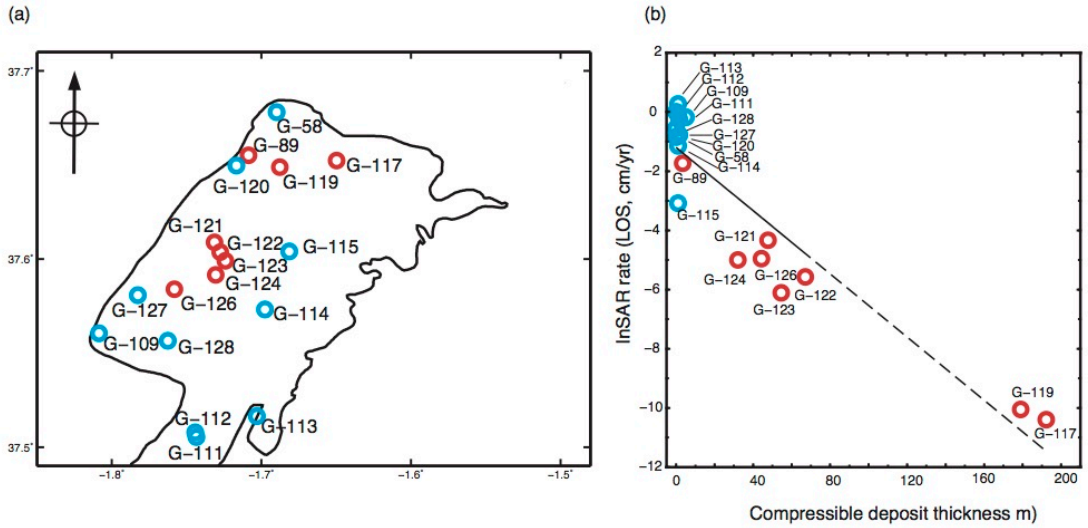

Figure S1. (**a**) Distribution of the 18 boreholes where the thickness of the compressible deposit was estimated by Boni et al. (2015). (**b**) Comparison between InSAR-derived deformation rate and compressible deposit thickness. Red circles in (**a**) and (**b**) represent boreholes with compressible deposit thickness greater than 1 m and blue circles in (**a**) and (**b**) represent boreholes with compressible deposit thickness lower or equal to 1 m.

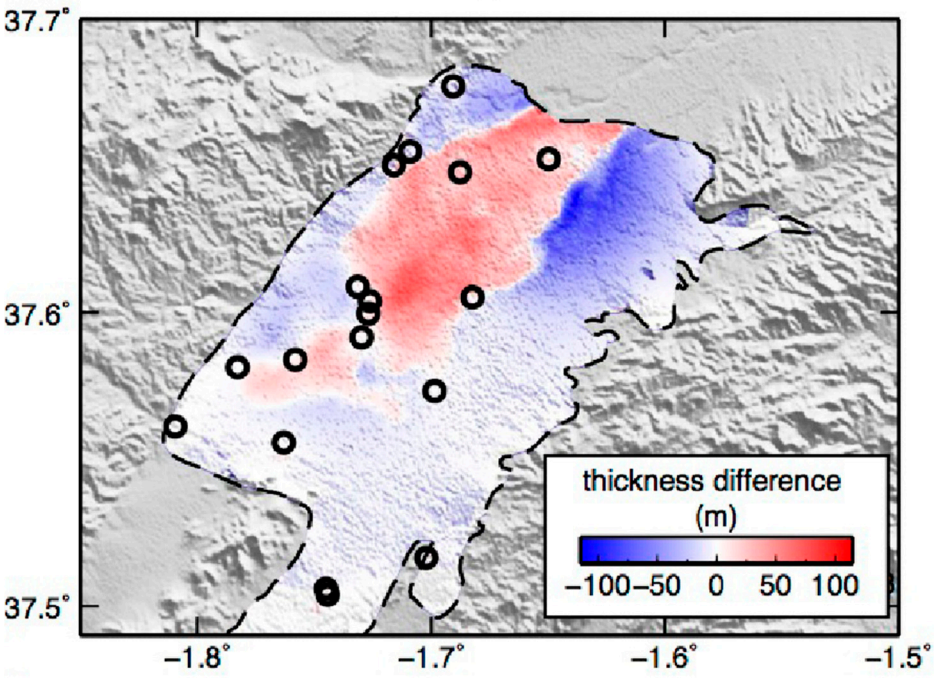

Figure A2. Map of residuals between the compressible deposit thickness map created in this study using the KED approach (Figure 6a) and the map created by Boni et al. (2015) using an ordinary kriging interpolation method (Figure 6b).

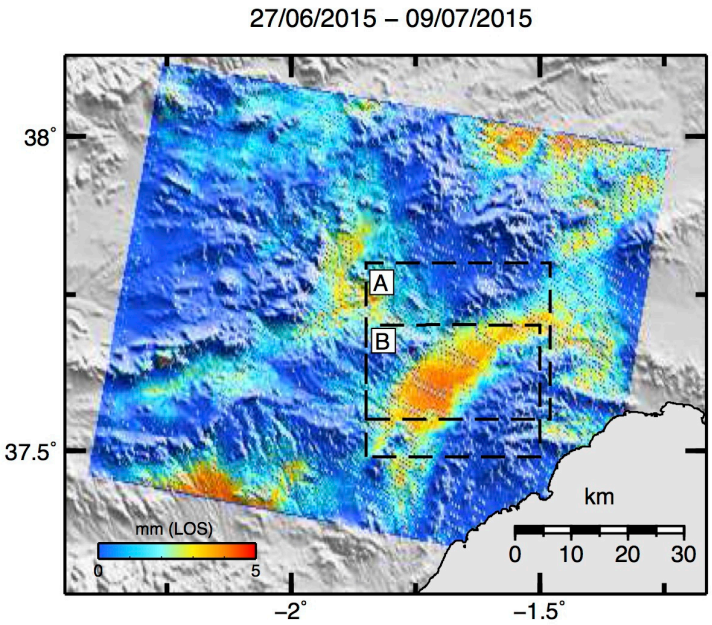

Figure A3. Sentinel-1 interferogram covering the period 27/06/2015–09/07/2015. This interferogram was created from two Sentinel-1A Interferometric Wide Swath images acquired in a descending orbit using the procedure described in Crosetto et al. (2011). The black-dashed rectangles labelled A and B outline the regions shown in Figure 2 and Figure 6, respectively.

References

1. Boni, R.; Herrera,G.; Meisina, C.; Notti, D.; Béjar-Pizarro, M.; Zucca, F.; González, P.J.; Palano, M.; Tomás,R.; Fernández, J. Twenty-year advanced DInSAR analysis of severe land subsidence: The Alto Guadalentín Basin (Spain) case study. *Eng. Geol.* **2015**, doi:10.1016/j.enggeo.2015.08.014.
2. Crosetto, M.; Monserrat, O.; Cuevas, M.; Crippa, B. Spaceborne differential SAR interferometry: data analysis tools for deformation measurement. *Remote Sens.* **2011**, *3*, 305–318.